Pisco Med Publishing

Study on Hydrotalcite-like Derived Zn-Ni-Al-Fe-O Catalyst for Auto-Thermal Reforming of Acetic Acid to Produce Hydrogen.

Jialiang Xu

Henan Diheng Energy Chemical Co., Ltd., xujl@piscomed.com

Abstract: $Zn_{2.4}$ $Ni_{0.6}$ $Al_xFe_{1-x}O_{4.5\pm\delta}$(x=1/0.5/0) series of hydrotalcite-like nickel-based catalysts were prepared by coprecipitation method, which were used for autothermal reforming of acetic acid to produce hydrogen. The catalysts were characterized by XRD, H2-TPR, BET, XPS and other characterization methods. The results showed that $Zn_{2.4}$ $Ni_{0.6}$ $Al_{0.5}$ $Fe_{0.5}$ $O_{4.5\pm\delta}$ conversion rate of acetic acid was maintained at 100% in autothermal reforming of acetic acid, and the hydrogen yield was 2. 39mol-H2/mol-HAc. The Zn-Al hydrotalcite precursor is roasted to form ZnO-based composite oxide. The addition of appropriate amount of iron increases the specific surface area of the catalyst. After reduction, FeNiZn alloy is formed. The electron donating effects of Fe and Zn improve the oxidation resistance of Ni, and the oxidation sintering and carbon deposit resistance of the catalyst are improved.

Keywords: FeNiZn alloy; Hydrotalcite-like nickel-based catalyst; Hydrogen Production by Autothermal Reforming of Acetic Acid

As a clean energy, hydrogen is a potential alternative to fossil energy [1]. Traditional hydrogen production methods often use fossil materials such as natural gas and coal, which often bring about environmental pollution [2]. The production of hydrogen from renewable biomass is currently a hot research topic for scientists all over the world [3], and biomass can be pyrolyzed at high temperature to obtain biomass oil, which contains oil phase and water phase components (acetic acid accounts for about 30%) [4], among which cheap water phase components can be used as hydrogen production raw materials. Acetic acid, a typical component of biomass oil, is often selected as the research object due to the complex composition of water phase components. Hydrogen production from acetic acid reforming generally includes steam reforming reaction (SR)($CH_3COOH+2H_2O\rightarrow 2CO_2+4H_2$), partial oxidation reaction (POX)($CH_3COOH+O_2\rightarrow 2CO_2+2H_2$) and autothermal reforming reaction (ATR)($CH_3COOH+xO_2+yH_2O\rightarrow aCO+bCO_2+cH_2$. Steam reforming hydrogen production usually uses excessive steam to improve acetic acid conversion rate and prevent catalyst carbon deposit deactivation, but steam reforming hydrogen production is a strong endothermic reaction with high energy consumption. The partial oxidation reaction is an exothermic reaction, which can realize self-heating and can be converted at a lower temperature (750-800 DEG C). However, in high oxygen atmosphere, the catalyst bed is often overheated locally, and the catalytic materials used should have good oxidation resistance. Moreover, excess oxygen will consume raw materials and reduce hydrogen yield [5, 6]. Autothermal reforming combines steam reforming and partial oxidation processes to balance the heat supply of the reaction system. However, the oxidizing atmosphere and high temperature in the autothermal reforming process also easily lead to the oxidation and sintering of the catalyst [4]. For example, Huang et al [7] studied the application of Al2O3-supported Ni-based and Co-based catalysts in autothermal reforming reaction. It was found that the temperature at the front end of the catalyst bed was as high as 1000℃, and the oxidation and sintering eventually led to the reduction of catalyst activity.

The oxidation and sintering problems of catalysts caused by oxidizing atmosphere and high temperature in the autothermal reforming process mentioned above can be solved by introducing stable structures and additives [8]. For example, Feng et al. [2] introduced the active component Ni into the olivine structure through hydrothermal synthesis, and found that H2 yield was high and stable, because the prepared olivine obtained high specific surface area and porous structure,

and the active component was not easy to sinter in high temperature environment after entering the catalyst framework.

Hydrotalcite (HT) has a typical layered structure, which is also known as layered bimetallic hydroxides (LDHs). The general structural formula is $[M(II)_{1-x}M(III)_x(OH)_2]^{x+}[A^{n}_{x}{}^{-}/_{n}\cdot mH_2O]^{x-}$. Wherein, M(II) represents divalent cation on the laminate, M(III) represents trivalent cation on the laminate, an-represents interlayer anion, x=M(III)/(M(II)+M(III)), the cation and interlayer anion on the laminate have adjustable denaturation, and the compound substituted by the same crystal of divalent or trivalent metal on the laminate is called hydrotalcite-like compound (HTLCs), typically Zn-Al hydrotalcite-like.

The composite oxide obtained from the Zn-Al hydrotalcite-like precursor after heat treatment can form a stable ZnO skeleton [9], can uniformly disperse active components, and has good sintering resistance. Joseph et al [10] found that stability mg < Mn < co ≈ Ni < Zn in divalent metals, while stability al < Fe in M(III). In addition, Li et al [11] studied the use of Ni-based Zn-Al hydrotalcite-like catalyst for hydrogenolysis of glycerol, and found that the Ni-Zn alloy can be formed by doping Zn into the crystal lattice of Ni, and the selectivity of 1, 2-propanediol is increased by two times.

In view of deactivation caused by oxidizing atmosphere in ATR process, Fe is added to Al_2O_3-supported Ni-based catalyst as auxiliary agent. Fe and Ni form NiFe alloy [4], which can effectively inhibit oxidation of active component Ni [12]. Bolshak et al. [13] found that Fe not only can be used as a structure promoter to improve the dispersibility of active metals, but also can be used as an electron donor to improve the reducibility and oxidation resistance of active components. Wang et al [14] found that Fe and Zn can produce synergistic effect and improve catalytic performance. The alkaline potential of the mixed oxide formed by roasting Fe and Zn can extract Hδ+ from methanol, thus effectively promoting the reaction between methanol and methyl carbamate to generate dimethyl carbonate.

Therefore, in this study, a hydrotalcite-like precursor $[(Zn/Ni)_{1-x}(Al/Fe)_x(OH)_2]^{x+}$ $[(CO_3)_{x/2}\cdot yH_2O]^{x-}$, was prepared by coprecipitation method using nickel-based catalyst and iron as an auxiliary agent, and the composite oxide Zn-Ni-Al-Fe-O was obtained after calcination. The composite oxide derived from the hydrotalcite-like structure has a ZnO framework, and the sintering resistance and the dispersibility of active components are enhanced. The specific surface area is increased by the addition of Fe. The electron donating effect of Fe and Zn improves the oxidation resistance of the catalyst, thus realizing better activity and stability of acetic acid autothermal reforming reaction.

1. Experimental Part

1.1 Preparation of Catalyst

In this study, Ni-based hydrotalcite catalysts were prepared by coprecipitation method. Nitrate solution of zinc, nickel, aluminum and iron is adopted, and according to Zn/Ni/al/Fe = 2. 4/0.6/x/(1-x) mass ratio (x = 1,0. 5, 0), the above four raw materials reagent and sodium carbonate and sodium hydroxide precipitation (carbonate ion/hydroxide ion =1/16, all metal cations/hydroxide ion = 1/8), the precipitation process pH value is maintained at 10. 5±0.5 aging for 18 hours at a constant temperature of 78℃ in a water bath. Wash the precipitate with deionized water for three times, dry at 105 DEG C for 24 hours, and roast at 700 DEG C for 4 hours to obtain composite oxide. Finally, the 20-40 mesh composite oxide catalyst is obtained by tabletting and sieving, as shown in Table 1.

Table 1 List of crystal sizes, partical size and BET data of the catalysts

Catalyst	Nominal compisitions	Surface area A/ ($m^2\cdot g^{-1}$)	Pore volume v/ ($cm^3\cdot g^{-1}$)	Average pore size d/nm	Particle size measured by XRD d/nm	
					reduced	spent
ZNA	$Zn_{2.4}Ni_{0.6}AlO_{4.5\pm\delta}$	40.0	0.146	12.3	16.0[a]	17.9[a]
$ZNA_{0.5}F_{0.5}$	$Zn_{2.4}Ni_{0.6}Al_{0.5}Fe_{0.5}O_{4.5\pm\delta}$	48.3	0.145	9.8	16.6[b]	16.1[b]
ZNF	$Zn_{2.4}Ni_{0.6}FeO_{4.5\pm\delta}$	31.2	0.088	10.2	22.6[b]	28.0[b]

[a]: 43.6° for NiZn alloy; [b]: 51.3° for NiFe alloy

1.2 Performance Evaluation of Catalysts

Autothermal reforming of acetic acid in quartz tube of continuous flow fixed bed(4mm) reactor. 0.2g catalyst

(particle size 20-40 mesh) are placed between Shi Ying cotton in that reactor in H2 atmosphere reduction treatment at 700℃ for 1h, and then the mixed solution of water and acetic acid was mixed in Gasification at 330℃ followed by mass ratio with O2 and N2n(CH_3COOH): n(H_2O): n(O_2): n(N_2)=1:4:0.28:3.92, airspeed 11250 ml/(gcatalysth), 650℃ and mix at quasi-atmospheric standard pressure, then the mixture entersthe reactor, and the reaction products are colored by gas phase Spectrum (SP-7890, Lunan instrument) was analyzed on line, N2 was used as internal standard gas. Acetic acid conversion rate (xHAc), carbon-containing product selectivity (si) and hydrogen yield (wH2) are obtained by the following formula:

$$x_{HAc} = \frac{F_{HAc,in} - F_{HAc,out}}{F_{HAc,in}} \quad (1)$$

$$s_i = \frac{F_i}{n_i (F_{HAc,in} - F_{HAc,out})} \quad (2)$$

$$w_{H_2} = \frac{F_{H_2,product}}{F_{HAc,in}} \quad (3)$$

In the above formula, $F_{i,in}$ and $F_{i,out}$ are the molar flow rates of substance i at the inlet and outlet of the reactor, and n_i is the stoichiometric factor of carbon-containing products and acetic acid.

1.3 Characterization of catalyst

X-ray diffraction characterization was performed on DX-2700 (Dandong Fangyuan Instrument), scanning at 5-80, tube current 30mA, tube voltage 40kV. The specific surface area, average pore diameter and pore volume of catalyst samples were analyzed by low temperature nitrogen physical adsorption method on JW-BK112 specific surface area and pore diameter analyzer (Beijing Jingwei Gaobo Instrument Company). X-ray photoelectron spectroscopy was tested on

KratosAxis-UltraDLD photoelectron spectrometer, with Al's Kα line as excitation source and C1s electron binding energy (284. 6eV) as internal standard correction.Thermogravimetric analysis was carried out with STA409PC(NETZSCH) thermogravimetric analyzer at a heating rate of 10℃/min.

2. Results and discussion

2.1 Activity Test of Acetic Acid Autothermal Reforming for Hydrogen Production

$Zn_{2.4}Ni_{0.6}Al_xFe_{1-x}O_{4.5\pm\delta}$ series catalysts are used in autothermal reforming of acetic acid. The results are shown in fig. 1 and $Zn_{2.4}Ni_{0.6}AlO_{4.5\pm\delta}$ in the activity test of the 5+-δ (ZNA) catalyst (fig. 1(a)), the hydrogen yield reduced from 2.31mol-H_2/mol-HAc to 0.63mol-H_2/mol-HAc, and the acetic acid conversion rate also decreased from nearly 100% at the beginning to 56. 3%. Correspondingly, the content of C2 and C3 by-products such as acetone increased from 13. 4% to 63. 2%。

$Zn_{2.4}Ni_{0.6}Al_{0.5}Fe_{0.5}O_{4.5\pm\delta}$($ZNA_{0.5}F_{0.5}$) formed after Fe was introduced in fig. 1(b), and the catalyst showed good activity and stability, and its hydrogen yield remained stable at 2.39mol-H_2/mol-HAc for 10 hours.The acetic acid conversion rate was maintained at about 100%, and the carbon dioxide selectivity was 60. 9%, carbon monoxide at 27. 3%, methane selectivity is 3. 9%. Figure 1 (c) $Zn_{2.4}Ni_{0.6}FeO_{4.5\pm\delta}$(ZNF) catalyst in the 10h activity test, the hydrogen yield decreased from 1.91mol-H_2/mol-HAc to 1.64mol-H_2/mol-HAc. The conversion of acetic acid also decreased to 94.7% after 5h; the selectivity of carbon dioxide was 43.1%, the selectivity of carbon monoxide was 42.7%, the selectivity of methane was stable at 6.5%, and by-products such as acetone and other C2 and C3. It increased from 5.8% to 10.6%. The reason for the difference in the activity and stability of the above catalysts is to be further characterized.

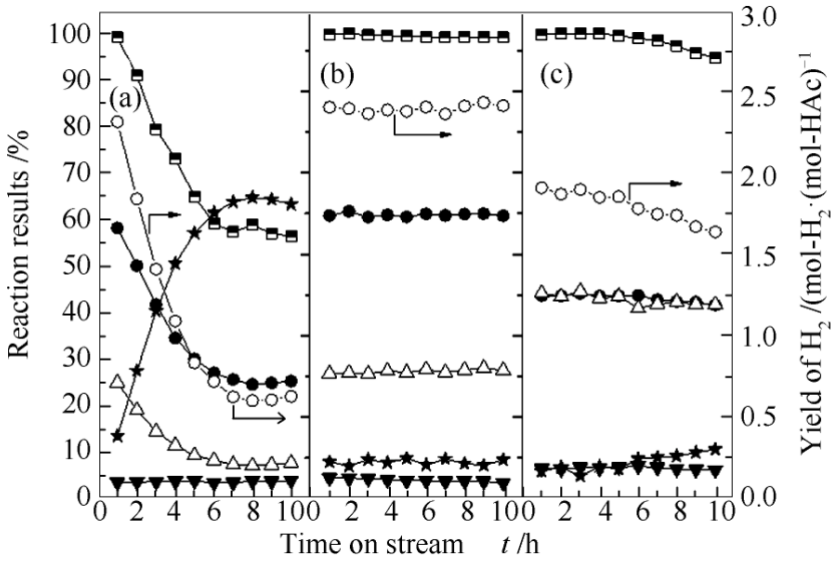

Figure1Catalytic performance of catalysts for ATR of HAc(a): ZNA; (b): ZNA0. 5 F0. 5; (c):ZNF

:xHAC; ●:sCO2; △:sCO; :sCH4; ★:sCH3COCH3; ○:wH2

In order to study the effect of O2 content on the catalyst, $ZNA_{0.5}F_{0.5}$, which had better performance in the activity test, was tested for different O_2/HAc, see fig. 2 for details.

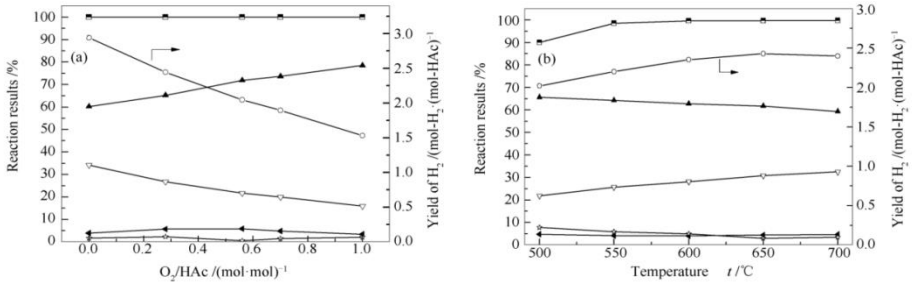

Figure2 Autothermal reforming reaction activity diagram of ZNA0.5F0.5 catalyst(a):ratiosofO2/HAc; (b):differenttemperatures

:xHAC; ▲:sCO2; :sCO; :sCH4; ☆:sCH3COCH3; ○:wH2

As can be seen from fig. 2(a), when n(O2)/n(HAc) is 0.28, the yield of H2 was 2. 43mol-H2/mol-HAc, which is close to the activity test result of fig. 1. With the increase of O2 content, the yield of H2 decreased obviously. When n(O2)/n(HAc)=1, the yield of H2 decreased to 1. 53mol-H2/mol-HAc. Therefore, considering autothermal reforming mode, n (O2)/n (HAC) = 0 is selected. 28 is appropriate.

As can be seen from fig. 2(b), when the reaction temperature is 700℃, the selectivity of carbon dioxide is 59. 3%, while the selectivity of carbon monoxide was higher, at 32. 3%. 5%; The yield of hydrogen was slightly lower, 2. 34mol-H2/mol-HAc, which may be caused by high temperature unfavorable to water-gas conversion reaction. When the reaction temperature is 650℃, the hydrogen yield is 2. 5%. 42mol-H2/mol-HAc, the selectivity of carbon dioxide and carbon monoxide are 57. 6% and 29. 8%. As the reaction temperature decreased to 500℃, the acetic acid conversion rate decreased to 90. 1%, the hydrogen yield also decreased to 2. 02mol-H2/mol-HAc, the selectivity of by-product acetone reached 19. 7%. The higher selectivity of acetone leads to $ZNA_{0.5}F_{0.5}$ catalyst has low activity at low temperature. Therefore, it is appropriate to choose 650℃ as the reaction temperature.

2.2 Characterization of catalyst

2.2.1 XRD Characterization of Precursor and Oxide

In order to understand the crystal phase structure change of Ni-based catalyst, the catalyst precursor was characterized by X-ray powder diffraction (XRD). Fig. 3(a) is an XRD spectrum of ZNAF series catalyst precursor. As shown in fig. 3(a), the ZNA catalyst precursor contains at 12. 4°, 24.2°, 39.8 degrees. The peaks are hydrotalcite-like structures (PDF-#:72-1100), while a small amount of ZnO structures (PDF-#:89-0510) appear. Chen et al. [15] found that when n(Zn)/n(Ni)=2. 4/0. 6=4＞2, excess Zn will form Zn(OH)2 and ZnO will be formed ZNA0 during aging. In the ZNA0.5F0.5 (Fig. 3(a)-b) and ZNF (Fig. 3(a)-c) in which Fe is gradually substituted for Al, the hydrotalcite-like structure peak gradually weakens, and the peak of the ZnO structure gradually increases and the peak shape changes sharply.

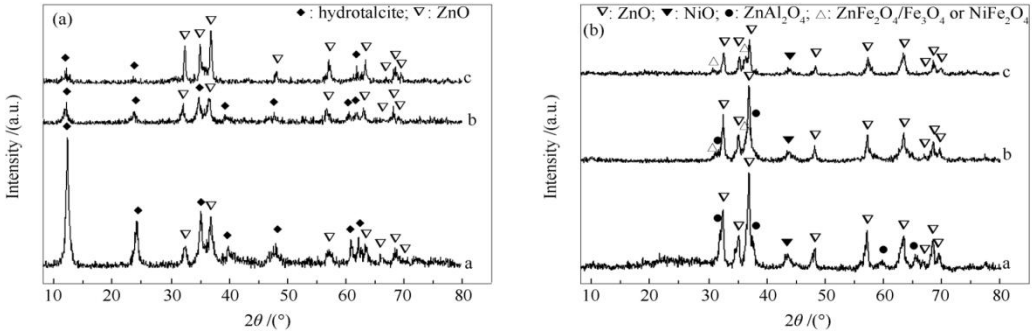

Fig. 3 x-ray powder diffraction pattern of 3ZNAF series catalyst

Fig. 3(b) is an XRD spectrum of oxides obtained by calcination of ZNAF series catalyst precursors at 700.℃ degree. After calcination at 700℃, the hydrotalcite-like structures of all catalysts disappeared. In ZNA (Figure 3(b)-a), there are mainly wurtzite ZnO(PDF-#:70-2551), spinel ZnAl2O4(PDF-#:81-0721) and NiO (PDF-#: 71-1179) [11]. In $ZNA_{0.5}F_{0.5}$(fig. 3(b)-b) catalyst, because of the introduction of Fe, at 30. 7℃, 36.3℃, new phases $ZnFe_2O_4/Fe_3O_4$ and $NiFe_2O_4$ (PDF-#:74-2397) were formed. In the ZNF in which Fe completely replaces Al (Fig. 3(b)-c), the spinel ZnAl2O4 phase disappears, and iron-containing spinel (ZnFe2O4/Fe3O4 and NiFe2O4) is formed at 30.7°, 36.3°, etc. Phase [7]

2.2.2 Characterization of Nitrogen Physical Adsorption

The specific surface area of oxide catalyst is measured by low temperature nitrogen physical adsorption. Fig. 4 is BET characterization of ZNAF series catalysts.

2.2.3 XRD Characterization of Catalyst after Reduction and Reaction

In order to study the state of the active components before the reaction, the catalyst was reduced at 700℃ for 1h and tested by XRD, as shown in fig. 5. As can be seen from fig. 5(a), ZnO(PDF-#:89-0510) phase is present in all catalysts. Ni-rich NiZn alloy (pdf-#: 87-0713) [11,16] phase is generated in ZNA (fig. 5(a)-a). In the ZNA0.5F0.5 (Fig. 5(a)-b) after the introduction of Fe, FeNiZn alloys were formed at 35.5°, 43.6°, 51.3° and 62.5° [4, 17], while NiO and ZnFe2O4/Fe3O4 and NiFe2O4 phases disappear. Similarly, in ZNF (fig. 5(a)-c) containing more Fe, the peak of iron-containing spinel (ZnFe2O4/Fe3O4 or NiFe2O4) also disappeared, and a stronger Fe-rich FeNiZn alloy diffraction peak was also formed [13]. In order to study the crystal phase transition during the reaction, XRD patterns of the catalyst after reaction at 650℃ for 10 hours were tested. As shown in fig. 5(b)-a, a carbon deposit peak (pdf-#: 75-2078) [18] appears at 26 degrees for the reacted ZNA. The original NiZn alloy phase disappeared and the weak peak of Ni (PDF-#:88-1715) was re-formed at 43.6° and 51.3°. The crystal phase was stable and did not change after the reaction of ZNA0.5F0.5 (Fig. 5(b)-b) and the reduced ZNA0.5F0.5 (Fig. 5(a)-b). ZNF (Fig. 5(b)-c) reacted for 10 h, and the iron-containing spinel (ZnFe2O4/Fe3O4 and NiFe2O4) phases appeared again, while the peak of the FeNiZn alloy phase became weak, indicating partial oxidation occurred. As shown in Table 1, the particle size of the active components of the ZNA and ZNF catalysts after the reaction increased, while the phase of the ZNA0.5F0.5 catalyst was stable and the particle size did not increase.

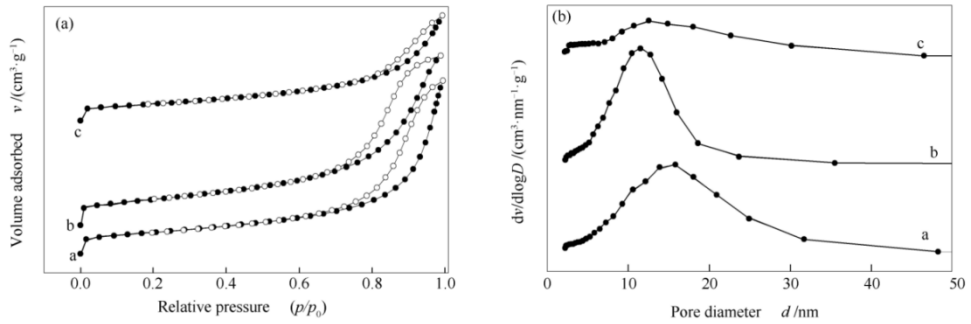

Figure4 BET of ZNAF catalysts (a):nitrogenadsorption-desorptionisotherms; (b):poresizedistributiona: ZNA; b: ZNA0. 5 F 0. 5; c:ZNF

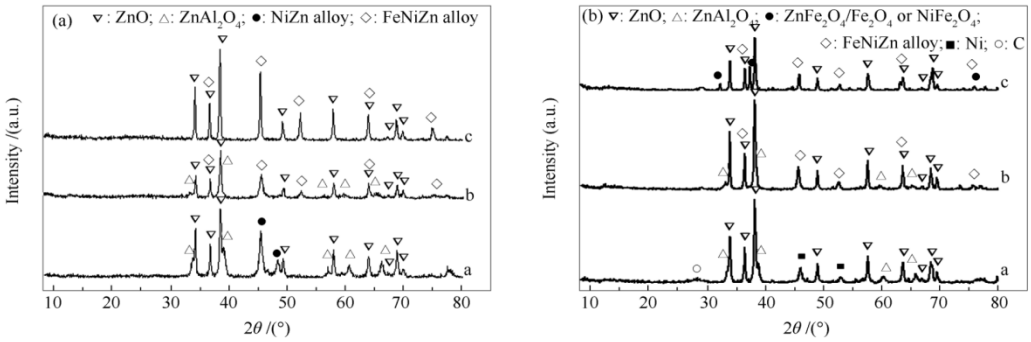

Figure5XR DpatternsofZNAFcatalysts(a):reduced; (b):spenta:ZNA; b:ZNA0. 5F0. 5; c:ZNF

2.2.4 X-ray photoelectron spectroscopy (XPS) characterization

XRD cannot identify amorphous Ni, while XPS can measure the surface electronic state of Ni atoms. It can be seen from the literature [12,19] that the XPS peak around 852eV is Ni2+ near Ni0,855 eV, while the peak around 861eV is Ni2+ oscillation companion peak. Semi-quantitative analysis shows that in the reduced zna-r catalyst (fig. 6(a)-a), n(Ni0)/n(Ni2++Ni0) is about 48. 1%, ZNA0. 5F0. In 5-r (fig. 6(a)-b), n(Ni0)/n(Ni2++Ni0) is about 17. 6%,

In znf-r (fig. 6(a)-c), n(Ni0)/n(Ni2++Ni0) is about 38. 0%。

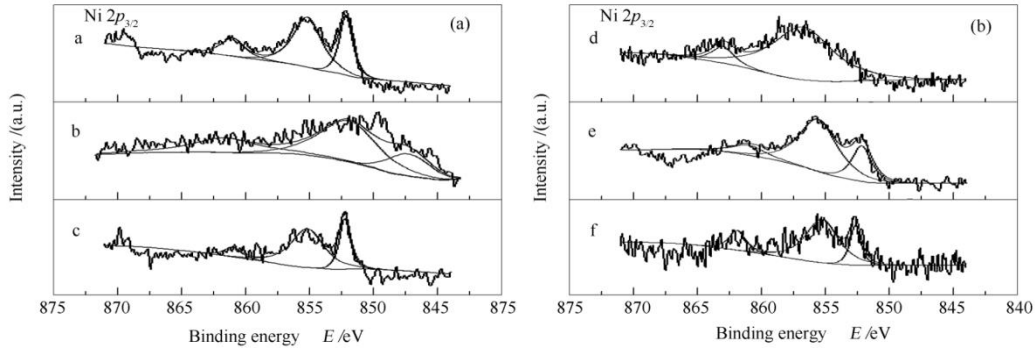

Fig. 6 photoelectron spectrum analysis of 6ZNAF series catalyst after reduction and reaction

(a)andspent(b)catalystsa:ZNA-R; b:ZNA0.5 F 0. 5-R; c: ZNF-R; d: ZNA-S; e: ZNA0.5 F0. 5-S; f: ZNF-S

In the ZNA-S catalyst after the reaction (fig. 6(b)-d), n(Ni0)/n(Ni2++Ni0) is about 5. 5%, ZNA0.5F0.5-S (fig. 6(b)-

e), n(Ni0)/n(Ni2++Ni0) is about 13. 4%, n(Ni0)/n(Ni2++Ni0) in ZNF-S (fig. 6(b)-f) is about 19. 5%. After the reaction, the ZNA catalyst n(Ni0)/n(Ni2++Ni0) decreased by 42. 6%, down significantly; ZNA0.5 F0.5.The change of n(Ni0)/n(Ni2++Ni0) before and after the reaction between 5 and ZNF catalysts is small.

2.2.5 TG/DTG characterization

In order to understand the carbon deposition of each catalyst after the reaction, TG/DTG characterization of the catalyst after the reaction is carried out, as shown in fig. 7. As can be seen from fig. 7, there are two weight loss peaks in all catalysts, of which the weight loss peak around 100℃ can be attributed to the loss of surface water. 653 in ZNA. The obvious weight loss at 2℃ can be attributed to carbon deposition gasification in ZNA catalyst [20], with a weight loss ratio of 17. 5%. 82%; ZNA0.5F0.626 in 5. The weight loss ratio of carbon deposit at 7℃ is 3. 87%; 645 in ZNF. The weight loss ratio of carbon deposit at 5℃ is 8. 68%. It can be seen that ZNA and ZNF catalysts are better than ZNA0. 5F0.5 after the reaction, carbon deposit appears [21], and the carbon deposit strength is zna > znf > zna0. 5F0.5.

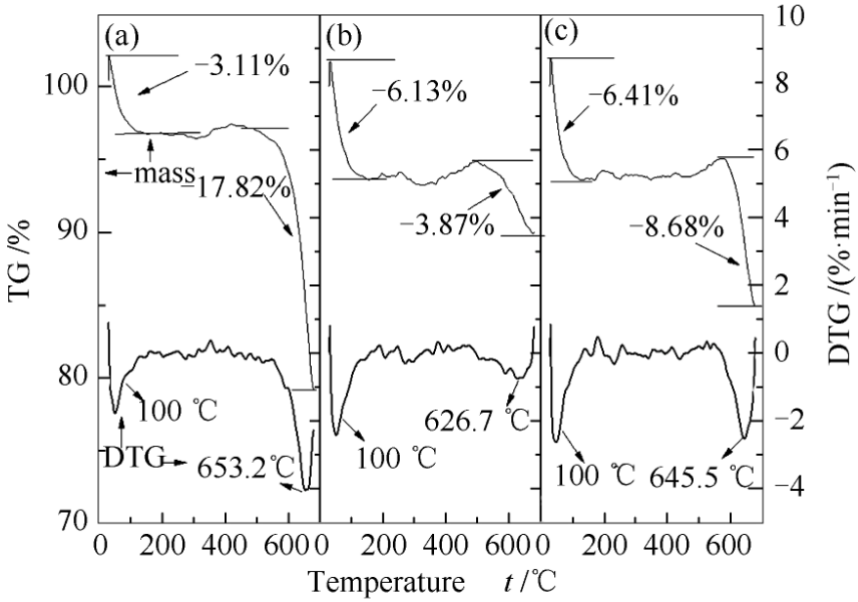

Fig. 7 thermogravimetric analysis of catalyst after 7ZNAF series reaction

(a) ZNA; (b): ZNA0.5F0.5; (c):ZNF

(a)

2.3 discussion

$Zn_{2.4}Ni_{0.6}AlO_{4.5\pm\delta}$(ZNA) catalyst was prepared by coprecipitation method. The precursor was mainly hydrotalcite-like structure with a small amount of ZnO. After calcination at 700℃, the hydrotalcite-like structure was transformed to ZnO as the main component, and ZnAl2O4 and NiO phases were formed at the same time. During the reduction process, due to the electron donating effect of Zn, the reduction of active component Ni was promoted [1], and XPS showed that the reduction degree of Ni reached 48. 1%, and NiZn alloy is formed after reduction. The particle size calculated by XRD is 16. 0nm. In the activity test, the acetic acid conversion rate of ZNA catalyst was close to 100% and the H2 yield reached 2. 5% at the initial stage of ATR reaction. 31mol-H2/mol-HAc. However, with the progress of the reaction, oxidation occurred, and XPS showed that n(Ni0)/n(Ni2++Ni0) decreased to 5. While the particle size did not change much, it was 17. 5%. 9nm. At the same time, XRD shows a carbon deposit peak at 26, while TG/DTG shows a carbon deposit weight loss rate of 17. 82%. Correspondingly, the acetic acid conversion rate of ZNA catalyst decreased to 56. 5% after 10 hours of reaction. 3%, H2 yield dropped sharply to 0. 5%. 63mol-H2/mol-HAc.

$Zn_{2.4}Ni_{0.6}A_{0.5}F_{0.5}O_{4.5\pm\delta}$($ZNA_{0.5}F_{0.5}$)formed after Fe was introduced. The catalyst, precursor forms hydrotalcite-like structure and a small amount of ZnO. After calcination, the hydrotalcite-like structure is transformed into a composite oxide with ZnO as the main body and spinel phase, including ZnAl2O4, ZnFe2O4/Fe3O4 or NiFe2O4 and NiO, and the specific surface area is increased to 48. 3m2/g, the most probable pore size is 10nm, and the pore size distribution is more concentrated, showing an improved degree of order. After reduction, XRD shows that Zn/Fe and active component Ni form FeNiZn alloy. The reduced $ZNA_{0.5}F_{0.5}$ in ATR reaction, H2 yield of catalyst 5 reached 2. 5%. 41mol-H2/mol-HAc and remained stable for 10 h. The reason for the stable reaction can be attributed to the formation of spinel structure by active components Ni and additives Al, Fe, etc., while the dispersion and blocking effect of ZnO skeleton in the catalyst on spinel has good thermal stability and improves the sintering resistance. NiFe alloy is formed after reduction, and the electron-donating effect of Fe [4] improves the oxidation resistance of the active component nickel in ATR atmosphere. Therefore, $ZNA_{0.5}F_{0.5}$ catalyst has stable crystal phase structure and stable valence state of active components before and after the reaction, thus showing higher activity and stability in the reaction.

For $Zn_{2.4}Ni_{0.6}FeO_{4.5\pm\delta}$(ZNF) catalyst, the precursor mainly forms ZnO structure. After calcination, a composite oxide structure of ZnO, spinel phase (ZnFe2O4/Fe3O4 or NiFe2O4) and NiO is formed. BET showed a specific surface area of 31. 2m2/g, the specific surface area decreased significantly. The acetic acid conversion rate of ZNF catalyst was 99. 9% at the initial stage of ATR reaction. The yield of H2 was 1. 5%. 91mol-H2/mol-HAc. After 10 hours of reaction, the acetic acid conversion of ZNF catalyst decreased to 94. 7%,

The yield of H2 dropped to 1. 64mol-H2/mol-HAc. The characterization results show that the active component Ni0 undergoes partial oxidation (the reduction degree is from 38. The figure dropped from 0% to 19. At the same time, partial sintering took place (particle size from 22. 5%. 6nm increased to 28. 0nm) and some carbon deposits (TG/DTG weight loss ratio is 8. 68%), resulting in slight deactivation of ZNF catalyst.

3. Conclusion

$Zn_{2.4}Ni_{0.6}AlO_{4.5\pm\delta}$, $Zn_{2.4}Ni_{0.6}Al_{0.5}Fe_{0.5}O_{4.5\pm\delta}$, $Zn_{2.4}Ni_{0.6}FeO_{4.5\pm\delta}$ catalyst derived from Zn-Al water slide stone was studied in this experiment. The results of characterization show that $Zn_{2.4}Ni_{0.6}AlO_{4.5\pm\delta}$ catalyst formed hydrotalcite-like structure and formed composite oxide structure after calcination. During autothermal reforming reaction, the active component Ni0 was oxidized and carbon deposit (TG/DTG) appeared, resulting in obvious deactivation. Fe replaces Al's $Zn_{2.4}Ni_{0.6}FeO_{4.5\pm\delta}$. The precursor of the 5+-δ catalyst is hydrotalcite and ZnO structure, and the composite oxide is obtained after roasting, and NiZnFe/NiFe alloy is formed after reduction, and the particle size of the NizNFE/NiFe alloy increases. During autothermal reforming, the active components undergo partial sintering and oxidation, resulting in the reduction of activity. And $Zn_{2.4}Ni_{0.6}Al_{0.5}Fl_{0.5}O_{4.5\pm\delta}$ catalyst has a large specific surface area. FeNiZn alloy with small particle size is formed after reduction, and remains stable in the reaction. No carbon deposit and other phenomena are found. Its hydrogen yield reaches 2.39mol-H_2/mol-HAc remained stable, indicating $Zn_{2.4}Ni_{0.6}Al_{0.5}Fl_{0.5}O_{4.5\pm\delta}$ catalyst has the characteristics of high activity, good stability, oxidation sintering resistance and carbon deposit resistance.

References

1. ZENGGM, LIUQH, GURX, ZHANGLH, LIYD. SynergyeffectofMgOandZnOina Ni/Mg-Zn-Alcatalystduringethanolsteamreformingfor H2-richgasproduction[J].CatalToday, 2011, 178(1):206－213.
2. FENGMH, LIUJD, ZHANGFB, HUANGLH. Ni-based olivine-type catalysts and theirapplication in hydrogenproductionviaauto-thermalreformingofaceticacid[J]. ChemPaper, 2015, 69(9).
3. HUANGLH, ZHANGFB, WANGN, CHENRR, HSUAT. Nickel-basedperovskitecatalysswithiron-dopingviaself-combustionforhydrogenproductioninauto-thermal reformingofethanol[J]. IntJHydroEnergy, 2012, 37(2):1272－1279.
4. ZHONGXY, XIEW, WANGN, DUANYP, SHANGRS, HUANGLH. Dolomite-deriveNi-basedcatalystswithFemodificationforhydrogenproductionviaauto-thermalreformingofaceticacid[J]. Catal, 2016, 6(6):85.
5. HUANGLH, ZHONGXY, DUANYP, XIEW, CHENRR. Preciousmetal-promoteNi-Mg-Al-Fe-Ocatalystforhydrogenproductionwithfaststartupviacatalyticpartialoxidationofbutanol[J]. IntJHydrogenEnergy, 2015. 40(4):1717－1725.
6. ZHANGFB, LIM, YANGL, YESZ, HUANGLH. Ni-Mg-Mn-Fe-Ocatalystderivedfromlayer

eddoublehydroxideforhydrogenproductionbyauto-thermalreformingofethanol[J]. CatalCommun, 2014, 43:6－10.
7. HUANGLH, LIUQ, CHENRR, HSUAT. Hydrogenproductionviaauto-thermalreformingof bio-ethanol:Theroleofironinlayereddoublehydroxide-derivedNi0. 35Mg2. 65AlO4. 5 ± δ catalysts[J]. ApplCatalA:Gen, 2011, 393(1/2):302－308.
8. Li Shuna, Shi Qi, Li Xiaojun, Fang Zhenhua, Sun Ping, Zhou Yuehua, Zhang Xingmei, Yang Xiaohui. Study on CO Low Temperature Oxidation Performance of Metal Doped Ce-M(M=Fe, Ni and Cu) Catalysts [J]. Journal of Fuel Chemistry, 2017,45 (6): 707-713.
9. ZHAOXF, ZHANGFZ, XUSL, EVANSDG, DUANX. FromlayereddoublehydroxidestoZnO-basedmixedmetaloxidesbythermaldecomposition:TransformationmechanismandUV-blockingpropertiesoftheproduct[J]. ChemMater, 2010, 22(13):3933－3942.
10. JOSEPHWB, PAULSB. Layereddoublehydroxidestability. 1.Relativestabilitiesoflayered doublehydroxidesandtheirsimplecounterparts[J]. ChemMater, 1999, 11:298－302.
11. LIXR, ZHANGC, CHENGHY, HELM, LINWW, YUYC, ZHAOFY. EffectofZndopingonthehydrogenolysisofglyceroloverZnNiAlcatalyst[J]. JMolCatalA:Chem, 2014, 395:1－6.
12. HUANGLH, XIEJ, CHENRR, CHUD, HSUAT. FepromotedNi-Ce/Al2O3inauto-thermalreformingofethanolforhydrogenproduction[J]. CatalLett, 2009, 130(3/4):432－439.
13. BOLSHAKE, ABELL S, MONTAN D. EthanolsteamreformingoverNi-Fe-basedhydrotalcites:Effectofironcontentandreactiontemperature[J]. IntJHydrogerEnergy, 2013, 38(14):5594－5604.
14. WANGDF, ZHANGXL, GAOYY, XIAOFK, WEIW, SUNYH. Synthesisofdimethylcarbonatefrommethylcarbamateandmethanoloverlanthanumcompounds[J]. FuelProcessTechnol, 2010, 91(9):1081－1086.
15. CHENGY, XUNG, LIXP, LIUQL, YANGHJ, LIWQ.Hydrogenproductionbyaqueous-phase reformingofethyleneglycoloveraNi/Zn/Alderivedhydrotalcitecatalyst[J]. RSCAdv, 2015, 5(74):60128－60134.
16. PANZY, WANGRJ, CHENJX. Deoxygenationofmethyllaurateasamodelcompoundon Ni-Znalloyandintermetalliccompoundcatalysts:Geometricandelectroniceffectsofoxophilic Zn[J]. ApplCatalB:Environ, 2018, 224:88－100.
17. HUANGLH, XIEJ, CHENRR, CHUD, CHUW, HSUA.Effectofirononduralbilityof nickel-basedcatalystsinauto-thermalreformingofethanolforhydrogenproduction[J].IntJHydrogenEnergy, 2008, 33(24):7448－7456. 1
18. MONTANARIT, SISANIM, NOCCHETTIM, VIVANIR, DELGADOMCH, RAMISG, BUSCAG,Zinc-alumi numhydrotalcites COSTANTINOU. asprecursorsofbasiccatalysts:Preparation, characterizationandstudyoftheactivationofmethanol[J]. CatalToday, 2010, 152(1/4):104－109.
19. VELUS, SUZUKIK, VIJAYARAJM, BARMANS, GOPINATHCS. InsituXPSinvestigations ofCu1xNixZnAl-mixedmetaloxidecatalystsusedintheoxidativesteamreformingofbio-ethanol[J]. ApplCatalB:Environ, 2005, 55(4):287－299.
20. HUANGLH, LIUQ, CHENRR, CHUD, HSUAT. LayereddoublehydroxidederivedCo0. 3Mg2. 7Al1-xFexO4. 5± δ catalystsforhydrogenproductionviaauto-thermalreformingofbio-ethanol[J]. CatalCommun, 2010, 12(1):40－45.
21. CHEFL, GRAYJT, HAS, MCEWENJS. Reducingreactiontemperature, steamrequirements, andcokeformationduringmethanesteamreformingusingelectricfields:Amicrokineticmodelingandexperimentalstudy[J]. ACSCatal, 2017, 7(10):6957－6968.